Reconstructing wave packets by quantum-state holography

I. Sh. Averbukh and M. Shapiro
Department of Chemical Physics, Weizmann Institute of Science, Rehovot 76100, Israel

C. Leichtle and W. P. Schleich
Abteilung für Quantenphysik, Universität Ulm, D-89069 Ulm, Germany

(Received 9 September 1998)

We analyze and further develop our method of quantum-state holography for reconstructing quantum superposition states in molecules or atoms [Phys. Rev. Lett. **80**, 1418 (1998)]. The technique is based on mixing the unknown *object state* with a known *reference state* generated in the same system by two delayed laser pulses, and detecting the total time- and frequency-integrated fluorescence as a function of the delay. The feasibility of the method is demonstrated by reconstructing various vibrational wave packets in sodium dimers. Both the cases of completely controlled and noisy relative phase between the laser pulses are considered. In the latter case, we use the technique of coherence observation by interference noise to recover the interference component of the fluorescence signal. Our results clearly demonstrate the robustness of quantum-state holography and the high quality of reconstruction even in the presence of the external noise. [S1050-2947(99)06403-3]

PACS number(s): 32.80.Qk, 42.50.Md, 03.65.Bz, 42.50.Lc

I. INTRODUCTION

The past few years have seen an upsurge of interest in the old problem of quantum-state preparation and measurement (see, for example, [1–5]). Quantum-state preparation deals with the creation of states of quantum fields or material systems in a *controlled* manner. On the other hand, the notion of ''measuring a state'' refers to a *series* of measurements on an *ensemble* of identically prepared systems whose outcomes contain all the necessary information to reconstruct the *complex*-valued wave function or density matrix of the system from *real*-valued experimental data. Consequently, *phase-sensitive* techniques must be employed to extract the full phase information of the quantum state of the system.

This is a difficult experimental task, and a complete determination of quantum states has been achieved for a few systems only. Among them are the measurement of the state of hydrogen formed in H^+-He collisions [6], of the electromagnetic radiation field via eight-port interferometry [7,8] and optical homodyne tomography [9,10], and of the vibratory motion of a single ion stored in a Paul trap [11]. Moreover, the motional quantum state of a cold atomic beam has been observed [12].

In this paper, we address the problem of measuring the quantum state of a molecule [13–19]. Dunn, Walmsley, and Mukamel have managed to recover experimentally a quasiclassical vibrational state of a sodium dimer with the help of *emission tomography* [13]: By measuring the time-dependent spectrum of the fluorescence of the molecule they were able to reconstruct a generalized phase-space distribution of a vibrational wave packet in Na_2. However, their scheme relies on several approximations which presume an essentially harmonic potential. Moreover, this scheme measures a smoothed version of the Wigner function and is therefore hardly capable of reconstructing highly nonclassical features, if such exist [17].

Leonhardt and Raymer have shown theoretically how to recover the quantum state of a one-dimensional wave packet in an arbitrary binding potential from its time-dependent position distributions [16]. Unfortunately, this quantity is not easy to measure experimentally. Moreover, for an anharmonic potential one has to monitor — at least in principle — the temporal evolution of the wave packet for a very long time. For example, for a Morse potential one has to measure [18] the position distribution up to half of the so-called revival time T_{rev} [20].

Many of these problems are overcome by the method of *wave function imaging* [14,15] which uses both the time-resolved and frequency-resolved fluorescence of the molecule. Relying on a basis set expansion it is possible to invert the above data to obtain the complex amplitudes of the contributing eigenstates which build up the wave packet. However, since the unknown coefficients enter the relevant algebraic equations quadratically, the method is highly sensitive to experimental noise.

In order to resolve this problem, we have recently developed [21] a new linear technique for the reconstruction of quantum superposition states (wave packets). Because of its linearity, it overcomes the shortcomings of the wave function imaging method. In common to this method, it is able to reconstruct even highly nonclassical states. The new method was termed ''quantum-state holography,'' as a natural generalization of optical holography to material waves.

In the present paper we describe in detail the method of quantum-state holography, and demonstrate its feasibility by numerically simulating the reconstruction of vibrational wave packets in sodium dimers. In particular, we study two realizations of the method, which use stable or noisy interferometers. In the latter case, the recently proposed technique of coherence observation by interference noise (COIN) [22,23] is utilized for a simple and robust implementation of quantum holography. Different inversion schemes are tested.

The organization of the paper is as follows: In Sec. II we outline the idea of quantum-state holography for the recon-

struction of molecular quantum states. We devote Sec. III to an application of this technique to the case of a stable interferometer and demonstrate its feasibility by numerically simulating the reconstruction of complicated coherent superposition states. We include random measurement errors to test the stability of our scheme and discuss the role of the reference state in the performance of quantum-state holography. In Sec. IV we generalize the method to treating noisy COIN interferometers and study the dependence of the reconstruction fidelity on the magnitude of experimental noise. We summarize the main results of the paper in Sec. V and discuss further potential applications of our method.

II. PRINCIPLES OF QUANTUM-STATE HOLOGRAPHY

Vibrational wave packets in molecules are typically prepared by femtosecond laser pulses. In order to ''design'' a specific wave packet (''wave packet engineering''), one has to ''tailor'' a pulse by an appropriate pulse shaping apparatus. Such *amplitude*—as well as *phase*—shaping of ultrafast laser pulses has been demonstrated in a number of recent experiments (see, e.g., [24–28]).

But how can we measure that the preparation pulse has indeed created the desired state? The recently introduced method of *quantum-state holography* [21] employs a second, time-delayed, pulse that generates a second wave packet using the same electronic transition as the first one. For weak and phase-coherent pulses, the second pulse effectively adds a *reference* wave packet to the *object* wave packet excited by the first pump pulse. The interference between the two wave packets contains the complete phase information of the object state, provided the reference state differs from the object state. In this sense the situation is similar to ordinary optical holography [29]. As the ''hologram'' we suggest to record the total *incoherent* fluorescence of the excited molecule for different delay times τ between the two excitation processes. Our reconstruction step uses a simple numerical procedure to extract the full amplitude and phase information from this time-domain hologram.

A possible experimental setup for quantum-state holography (see Fig. 1) resembles that used in the technique of wave packet *cross* interferometry [26,30]. A single laser pulse is split into two identical pulses by a beam splitter. They are then introduced into the two arms of a Michelson interferometer. In one arm of the interferometer a pulse shaping apparatus is introduced which changes the amplitude and/or phases of the pump pulse I, whereas probe pulse II remains unchanged. After recombining the two pulses they excite subsequently the object and the reference wave packets in the molecules, whose incoherent fluorescence is detected. The length of the second arm may be varied with the help of a movable mirror to change the delay τ between the two pulses.

In contrast to wave packet autointerferometry [31], wave packet cross interferometry utilizes two *different* laser pulses, which in turn create *different* object and reference wave packets. The object state

$$|\psi_o(\tau)\rangle=\sum_n a_n e^{-i\omega_n\tau}|n\rangle \tag{1}$$

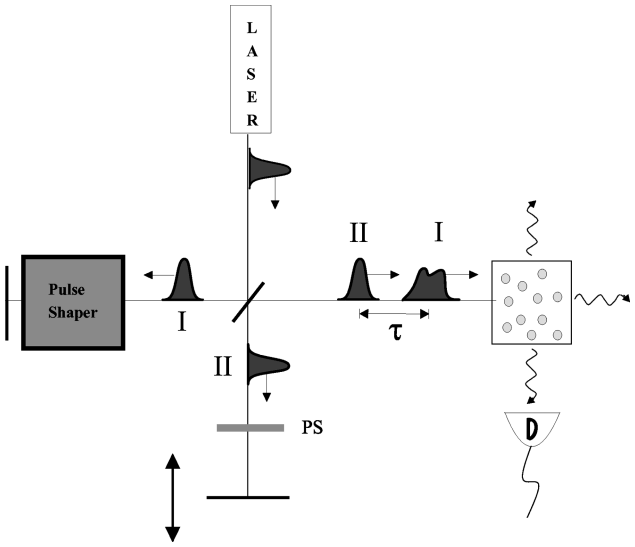

FIG. 1. Sketch of an experimental setup for quantum-state holography. A laser system delivers a short pulse which is split by a beam splitter into two identical replicas. These pulses are then introduced into two arms of a Michelson interferometer. The pump pulse I becomes ''tailored'' by a pulse-shaping apparatus and excites a desired *object* wave packet which we want to measure. The probe pulse II remains unchanged and excites a *reference* wave packet, which is added coherently to the object wave packet after a delay τ. As the ''hologram'' we detect the total fluorescence of the excited molecules as a function of the delay between the two pulses, which we vary with the help of a movable mirror. Since the fluorescence depends on the interference between the object and the reference wave packet, it contains the full phase information of the two quantum states in the superposition. Hence it can be used for the reconstruction of the quantum state of the object wave packet. Moreover, the phase shifter PS allows to change the overall relative phase between the pump and the probe pulse.

has already evolved in time for a period τ (corresponding to the delay time between the two pulses), when the reference state

$$|\psi_r\rangle=e^{i\phi(\tau)}\sum_n b_n|n\rangle \tag{2}$$

is being excited. Here $|n\rangle$ denotes the nth vibrational state with energy $E_n=\hbar\omega_n$ in the excited electronic level. In Eq. (2) we allow for an additional phase $\phi(\tau)$ between the object and reference wave packets. This relative phase is determined by the actual experimental setup and may depend on the delay time τ.

In the weak-field limit, the quantum state of the molecule reads

$$|\psi_{\rm tot}\rangle=|\psi_o\rangle+|\psi_r\rangle. \tag{3}$$

Hence, the probability P_n that the nth vibrational level of the superposition is populated follows as

$$P_n(\tau)=|a_n|^2+|b_n|^2+2\,{\rm Re}\{a_n b_n^* e^{-i[\omega_n\tau+\phi(\tau)]}\}. \tag{4}$$

It therefore depends on the delay time τ via the interference between the two wave packets.

Quantum-state holography relies on the observation that the interference term in Eq. (4) depends on the complex state *amplitudes* a_n and b_n, and not just on the *probabilities* $|a_n|^2$ and $|b_n|^2$. In analogy to ordinary holography the population P_n (which should be associated with the photographic density) allows for a full reconstruction of the object wave function.

However, there is no need to determine the population P_n for each of the states separately. It suffices to measure the time- and frequency-integrated fluorescence of the molecule making a spontaneous transition to the lower electronic level as a function of the delay time τ. For a wave packet comprised of several vibrational states $|n\rangle$ populated with probability P_n, the time-integrated energy emitted incoherently by the molecule is given by

$$F_{\rm tot}=\mathcal{F}\sum_{f,n} P_n|\langle f|n\rangle|^2\omega_{n,f}^4. \tag{5}$$

Here f designates the vibrational levels of the lower electronic state, $\omega_{n,f}=(E_n-E_f)/\hbar$ denotes the frequency difference of the two states, and $\mathcal{F}$ is a (positive) proportionality constant.

From Eqs. (4) and (5) it follows that the total fluorescence

$$F_{\rm tot}(\tau)=F_o+F_r+F_{\rm int}(\tau) \tag{6}$$

consists of the τ-independent terms

$$F_o\equiv\sum_n |\tilde{a}_n|^2 \tag{7}$$

and

$$F_r\equiv\sum_n |\tilde{b}_n|^2, \tag{8}$$

and the τ-dependent interference term

$$F_{\rm int}(\tau)\equiv 2\,{\rm Re}\left\{\sum_n \tilde{b}_n^*\tilde{a}_n e^{-i[\omega_n\tau+\phi(\tau)]}\right\}, \tag{9}$$

which results from the overlap between the two wave packets. Here we have used the notation

$$\tilde{a}_n\equiv a_n\sqrt{\mathcal{F}\sum_f |\langle f|n\rangle|^2\omega_{n,f}^4} \tag{10}$$

and

$$\tilde{b}_n\equiv b_n\sqrt{\mathcal{F}\sum_f |\langle f|n\rangle|^2\omega_{n,f}^4}. \tag{11}$$

Note that by measuring the fluorescence of the object and the reference wave packet separately, we find the quantities F_o and F_r, respectively. Hence we can distill the interference term $F_{\rm int}(\tau)$ from the total fluorescence $F_{\rm tot}(\tau)$ by subtracting F_o and F_r from $F_{\rm tot}(\tau)$. In the remainder we therefore concentrate on $F_{\rm int}(\tau)$ only.

We now show how to reconstruct the complete quantum state of the object wave packet from the measured signal $F_{\rm int}(\tau)$. For sufficiently short pulses, the Franck-Condon principle ensures that the excited wave function is just a replica of the vibrational state in the lower potential. We make use of this fact and employ such a short pulse to excite the reference wave packet. We emphasize that except of the shortness of this pulse no detailed knowledge about its phase and amplitude characteristics is needed.

When the molecule is initially in the eigenstate $|f\rangle$ in the lower electronic potential, the amplitudes b_n of the excited reference wave packet read therefore simply $b_n\propto\langle n|f\rangle$. From knowledge of these amplitudes we calculate the quantities $\tilde{b}_n$ via Eq. (11). Hence the only unknowns which enter the expression (9) for the fluorescence $F_{\rm int}(\tau)$ are the state amplitudes a_n for the unknown object wave packet. In the next two sections we develop two convenient inversion algorithms for extracting the complex-valued numbers a_n from the measured signal $F_{\rm int}(\tau)$. In this context, we distinguish the two cases of a stable and a noisy (COIN) interferometer.

III. HOLOGRAPHY WITH A STABLE INTERFEROMETER

In this section we analyze of quantum-state holography using a stable Michelson interferometer to prepare the sequence of the two laser pulses. In this case the pulses have a well-defined relative phase ϕ.

During the coherent interaction of the pulses with the molecule this relative phase ϕ is transferred onto the wave packets. If this relative phase is not locked, it just corresponds to the geometric path difference between the two arms of the interferometer and therefore reads

$$\phi(\tau)\equiv\phi_0+\omega_L\tau. \tag{12}$$

Here we allow for an additional phase shift ϕ_0 as in the experiments reported in Refs. [32,33]. In Fig. 1 this phase ϕ_0 is controlled by the phase shifter PS.

A. Inversion method

We now measure the fluorescence $F_{\rm int}(\tau)$ at a given delay τ for two different phase angles ϕ_0, e.g., $\phi_0=0$ and $\phi_0=-\pi/2$, and define the signal as

$$S(\tau)\equiv\frac{1}{2}\{F_{\rm int}(\tau,\phi_0=0)+iF_{\rm int}(\tau,\phi_0=-\pi/2)\}$$

$$=\sum_n \tilde{a}_n\tilde{b}_n^* e^{-i(\omega_n+\omega_L)\tau}. \tag{13}$$

Signals of this kind were measured in experiments [32] and [34].

Since every physical state characterized by the coefficients a_n is normalizable, these coefficients become negligible for a sufficiently large index n. Therefore we assume that the state to be reconstructed can be characterized by only a limited number of coefficients a_n with $n=0,\ldots,n_{\rm max}$. The quantity $n_{\rm max}$ is a free parameter of the reconstruction procedure, which has to be chosen large enough to ensure the accuracy of the procedure. We make at least $N=n_{\rm max}+1$ measurements of the signal $S(\tau)$ at distinct times τ_ν, $\nu=1,\ldots,N$, and write the resulting set of equations in matrix form

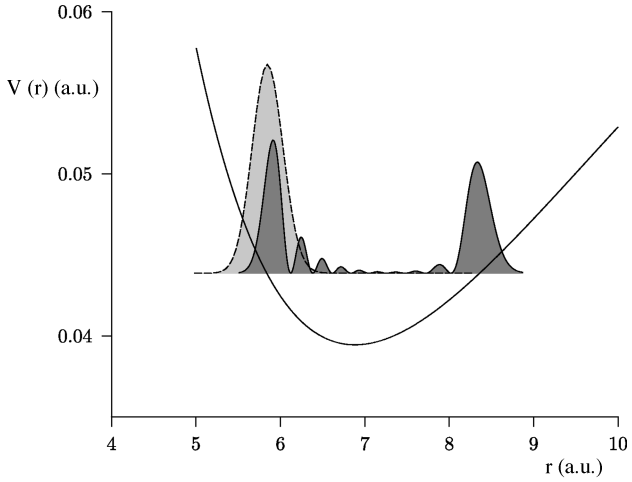

FIG. 2. Vibrational Schrödinger cat state in the excited Born-Oppenheimer potential of Na_2. The dark-shaded curve depicts the probability density of this state with amplitudes a_n given by Eq. (16). Note that the density has two dominant peaks at the left and right classical turning points of the underlying potential. The light-shaded curve shows the vibrational ground state $|g\rangle$ of the lower Born-Oppenheimer potential. In our reconstruction scheme we use this state as the reference state.

$$S(\tau_\nu)=\sum_{n=0}^{n_{\max}} e_{\nu,n}\tilde{a}_n, \tag{14}$$

where we have used the notation

$$e_{\nu,n}\equiv\tilde{b}_n^* e^{-i(\omega_n+\omega_L)\tau_\nu}. \tag{15}$$

By numerically inverting the set of equations (14) we can extract the quantities $\tilde{a}_n$ and from these we calculate the complex coefficients a_n via Eq. (10). In this way we are able to reconstruct the amplitudes a_n of the object wave packet in their moduli *and* phases.

For the inversion of the set of equations (14) it is convenient to use the method of *singular value decomposition*. This method allows us to invert square as well as rectangular (which corresponds to an overdetermined set of equations) matrices, even when the matrix is (almost) singular. For a detailed discussion, see, for example, Ref. [35]. We emphasize that our reconstruction scheme is numerically robust, since the unknown coefficients a_n enter the set of equations (14) linearly.

B. Example: Reconstruction of a vibrational Schrödinger cat state

We now demonstrate the feasibility of quantum-state holography using two states $X(^1\Sigma_g^+)$ and $A(^1\Sigma_u^+)$ of the sodium dimer, for which the potential curves are well known [36]. We calculate numerically the corresponding vibrational eigenstates and energies by the renormalized Numerov method [37]. As the object state we choose a molecular Schrödinger cat state [38,39] prepared in the upper electronic potential (see Fig. 2). Schrödinger cat states were created only recently in Rydberg atoms [33], for a single ion stored in the Paul trap [40], and for the electromagnetic field in a cavity [41].

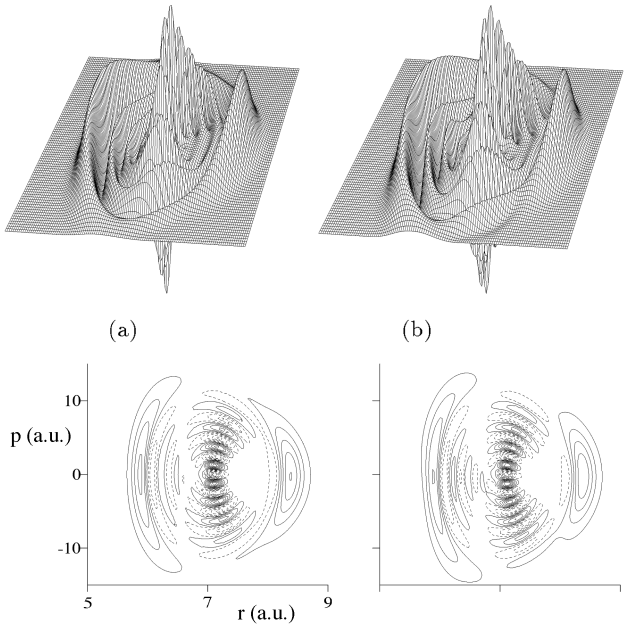

FIG. 3. Quantum-state holography of a Schrödinger cat state. In the bottom we show the contour lines of the Wigner functions displayed in the top. Here solid lines correspond to positive values and dashed lines to negative values, respectively. In (a) we present the exact Wigner function of the superposition state we want to measure. In (b) we show the reconstructed Wigner function, which exhibits all the nonclassical features of this state. We emphasize the excellent agreement between exact and reconstructed state despite the presence of simulated experimental measurement errors. This demonstrates the robustness of quantum-state holography.

A molecular Schrödinger cat state consists of a coherent superposition of two vibrational wave packets and can be excited by a pair of laser pulses (delayed in time by δt), which pump the system from the ground vibrational level $|g\rangle$. The probability amplitudes of the excited vibrational states are given by

$$a_n=\mathcal{N}\langle n|g\rangle\exp\left(-\frac{\Delta_n^2\Delta_t^2}{2}\right)\{1+e^{-i\Delta_n\delta t}\}. \tag{16}$$

Here $\mathcal{N}$ is a normalization constant and $\Delta_n\equiv\omega_n-\omega_g-\omega_L$ denotes the detuning for the nth level. The carrier frequency ω_L of the laser is chosen to be in resonance with the absorption maximum close to the $n=8$ state. As the initial state of the molecule we take the ground state $|g\rangle\equiv|f=0\rangle$ of the lower potential. We assume both laser pulses to have a Gaussian shape of duration Δ_t. For the numerical values of Δ_t and δt we use $\Delta_t=0.1T_{\rm vib}$ and $\delta t=0.5T_{\rm vib}$, where $T_{\rm vib}$ is the vibrational period. For this specified group of levels we have $T_{\rm vib}=300$ fsec. As the reference state we use the ground state $|g\rangle$ of the molecule.

In Fig. 3(a) we show the Wigner function [42]

$$W(r,p)=\frac{1}{\pi\hbar}\int_{-\infty}^{\infty}dy\,\psi^*(r-y)\psi(r+y)e^{-i2yp/\hbar} \tag{17}$$

of the state we wish to reconstruct. Here ψ is the wave function in coordinate space corresponding to the state with the expansion coefficients a_n, Eq. (16). Solid lines correspond

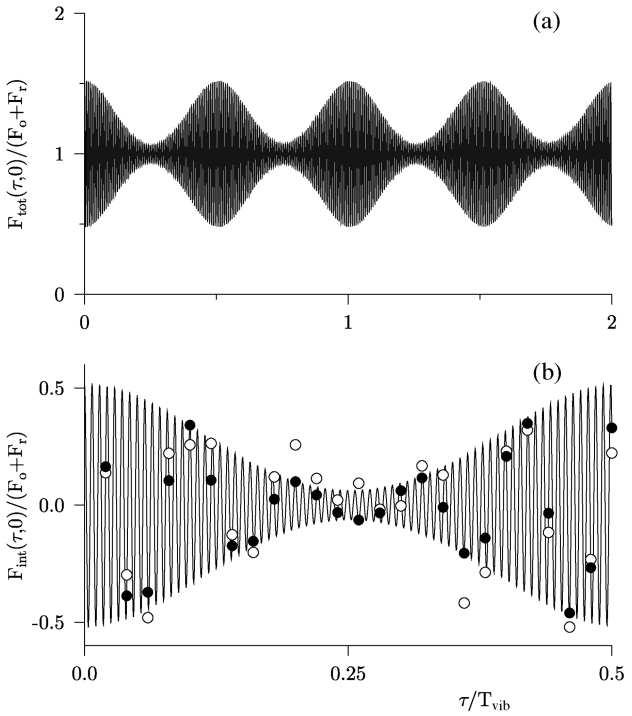

FIG. 4. Fluorescence hologram of a Schrödinger cat state. In (a) we show the total fluorescence as a function of the delay τ between the object and the reference pulses for the complete time region used for the reconstruction. In (b) we display the interference contribution to this total fluorescence for a small window around $\tau = T_{vib}/4$. Here we depict by white circles the simulated data points including measurement errors at the discrete times τ_ν, whereas the exact values at τ_ν are shown by black circles.

to positive values of the Wigner function and dashed lines correspond to negative values. From this figure we recognize that indeed this state consists of two distinct wave packets. The prominent fringe structure between the two centers of the wave packets is caused by the quantum interference between the two parts of the superposition state and hence shows the nonclassical features of this state.

In Fig. 4(a) we show the fluorescence hologram for the superposition state, Eq. (16), for the interval $\tau=0$ to $\tau = 2T_{vib}$. We note fast oscillations with the optical laser frequency ω_L and a slow modulation of the envelope which varies with a period of about $T_{vib}/2$. This behavior becomes clear if we recall that the superposition state shown in Fig. 2 consists actually of two wave packets originally centered at the left and right turning points of the potential. These two wave packets oscillate out of phase for a time τ until they interfere with the reference wave packet. Since the reference wave packet becomes excited at the left-turning point, the interference between the object wave packets and this reference wave packet takes only place near the Franck-Condon region. Hence we find the strongest variation of the fluorescence at multiples of half of the vibrational period.

In order to simulate errors of an actual measurement and to test the robustness of the reconstruction procedure, we introduce random fluctuations around the exact signal which obey a (normalized) Gaussian distribution with standard deviation σ. Here, we have chosen the value $\sigma=0.1(F_0+F_r)$ and have taken $N=100$ simulated data points at the discrete values τ_ν equally spaced between $\tau=0$ and $\tau=2T_{vib}$. In the bottom of Fig. 4 we magnify a small time window centered around the delay time $\tau=T_{vib}/4$. The simulated data points at the discrete times τ_ν are shown by white circles. In order to guide the eye we have marked the exact signal at the discrete times τ_ν by black circles.

Figure 3(b) presents the Wigner function of the reconstructed superposition state. A comparison with Fig. 3(a) demonstrates that the reconstruction reproduces nicely the exact state with all its phase-sensitive features despite the incorporation of measurement uncertainties.

As a measure for the fidelity of the reconstruction we use the overlap integral

$$o \equiv \left| \sum_n a_n^* a_n^{(\mathrm{rec})} \right| \tag{18}$$

between the exact state

$$|\psi_o\rangle = \sum_n a_n |n\rangle \tag{19}$$

and the reconstructed state

$$|\psi_o^{(\mathrm{rec})}\rangle = \sum_n a_n^{(\mathrm{rec})} |n\rangle. \tag{20}$$

An excellent fidelity with $o=0.98$ is obtained in this case.

C. Role of the reference state

In the above example we have used the vibrational ground state as the reference state. In this section we discuss the role of the reference state

$$|\psi_r\rangle = \sum_n b_n |n\rangle \tag{21}$$

in the performance of quantum-state holography. For this purpose we reconstruct the squeezed, rotated, and displaced state [43]

$$\psi(r) = \frac{1}{\sqrt[4]{\pi u}} \exp\left[i p_0 \frac{(r - r_0/2)}{\hbar} \right] \exp\left[-(1 - iv) \frac{(r - r_0)^2}{2u} \right], \tag{22}$$

whose Wigner function is shown in Fig. 5(a). Here we use the parameters $u=0.025$ a.u., $p_0=5$ a.u., $r_0=6$ a.u., and $v=2.1$. Such a state can be created by different methods (see, for example, Ref. [44], and references therein). Again we incorporate measurement errors, that is, the simulated data of the measurement fluctuate around the exact value according to a Gaussian distribution with variance $\sigma = 0.1(F_o+F_r)$. Moreover, we have chosen $N=200$ simulated data points equally spaced between $\tau=0$ and $\tau = 2T_{vib}$.

In Fig. 5(b) we show the Wigner function of the reconstructed state, when we use the vibrational ground state $|g\rangle = |f=0\rangle$ of the ground Born-Oppenheimer potential as the reference state. A comparison with the exact Wigner function shows that in this case the reconstruction was only par-

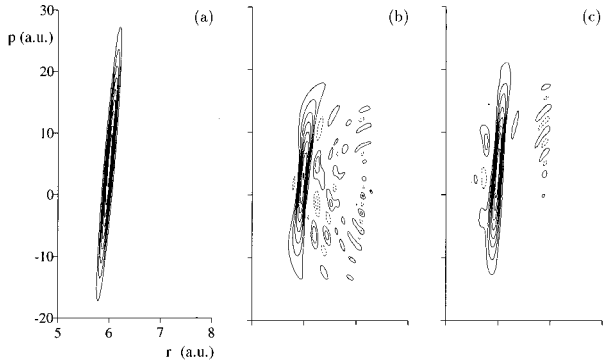

FIG. 5. The role of the reference state in the performance of quantum-state holography. In (a) we show the contour lines of the exact Wigner function of a rotated and displaced squeezed state, whereas in (b) and (c) we show reconstructed states. For the reconstruction in (b) and (c) we use the ground state $|f=0\rangle$ and the excited state $|f=4\rangle$ of the ground Born-Oppenheimer potential, respectively. In both cases the simulated fluorescence data incorporate measurement errors. We recognize that the quality of the reconstruction in (c) is better compared to (b). This shows that for this object state the reference state $|f=4\rangle$ is more suitable than the reference state $|f=0\rangle$.

tially successful. Although the main features of the state could be recovered, the wings of the reconstructed Wigner distribution differ from the exact one. This is an indication that coefficients a_n with large values of n corresponding to higher energies were discriminated in the reconstruction. This feature can be understood as follows.

From Eq. (9) we find that only those states $|n\rangle$ contribute to the fluorescence signal for which the amplitudes of *both* the signal state a_n *and* the reference state b_n are nonzero. Hence in order to reconstruct all contributing amplitudes a_n which build up the quantum state to be measured, the reference wave packet has to cover the complete energy range populated by the coefficients a_n. In the present example, however, the amplitudes b_n for the reference state $|f=0\rangle$ fall off too rapidly for large n as can be seen from Fig. 6. In this graph we show the probabilities $P_n=|a_n|^2$ for the squeezed state, Eq. (22), together with the probabilities $P_n=|b_n|^2$ for

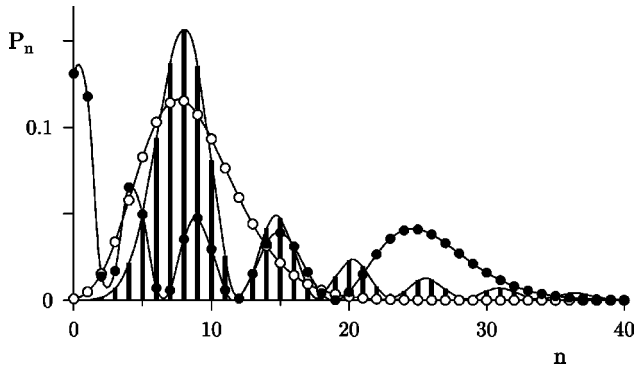

FIG. 6. The population P_n of the nth energy state for a rotated and displaced squeezed state and different reference states. We display the values of $P_n=|a_n|^2$ for the squeezed state by bars. In contrast, the probabilities $P_n=|b_n|^2$ for the two reference states $|f=0\rangle$ and $|f=4\rangle$ are depicted by white and black circles, respectively. To guide the eye we have connected the discrete values by continuous curves.

two different reference states, namely, the eigenstates $|f=0\rangle$ and $|f=4\rangle$ of the ground Born-Oppenheimer potential. Whereas the $|f=0\rangle$ reference state does not cover the complete energy region spanned by the squeezed state, the $|f=4\rangle$ state does. Hence, for the reconstruction of the squeezed state, Eq. (22), the reference state $|f=4\rangle$ seems to be more suitable.

In Fig. 5(c) we show the Wigner function of the squeezed state reconstructed with the help of the reference state $|f=4\rangle$. Again measurement errors were included in the simulation in the same manner as done before. Indeed, we find in this case a better agreement between the exact and the reconstructed Wigner function. Here, the fidelity parameter is $o=0.94$ in contrast to the value $o=0.87$ for the reference state $|f=0\rangle$.

IV. COIN HOLOGRAPHY

In the last section we have assumed that the interferometer used to produce the sequence of object and reference pulses is stable in the sense that the relative phase ϕ between the two pulses is reproducible in each run of the experiment for a fixed delay τ between the pulses. If, however, a pulse shaper is introduced into one arm of the interferometer, this may be a very demanding experimental task, especially if this arm becomes very long due to the pulse shaping apparatus [26].

The first experiments on wave packet interferometry [31] exercised a precise control of the relative phase by phase locking the two laser pulses. In Refs. [45–47] a different phase-sensitive technique was used. The presence of a strong phase noise washes out all the interference components from the time-averaged signal, thereby seemingly preventing the use of incoherent pulses for wave packet interferometry.

The new technique [22] of coherence observation by interference noise shows that the above statement is not necessarily true. The COIN technique concentrates on *fluctuations* in the population excited by a pair of time-delayed *randomly phased* pulses. Although the interference component is not present in the *mean* signal, the effect of interferences can still be felt by measuring the *fluctuations* of the signal about its mean value [22,23]. For example, when the two excitation pathways interfere strongly, fluctuations of the relative phase between the pump and probe pulses give rise to large fluctuations in the observed signal. Conversely, when the processes are independent of each other one merely observes the ''mean'' degree of fluctuations. The COIN technique has been experimentally demonstrated both for atomic [22,48] and molecular [49] systems (see also [50]). The method possesses interferometric sensitivity without stringent stability requirements on the system.

In the presence of noise the relative phase ϕ between the two laser pulses is a stochastic quantity and may therefore vary for different runs of the experiment at a fixed delay time τ. Since the coherent interaction of the two pulses with the molecule maps this relative phase onto the relative phase between the two excited wave packets, the quantity $F_{\rm int}(\tau)$ becomes a stochastic quantity. In contrast to the delay-independent contributions F_r and F_o the interference term depends on ϕ, that is, $F_{\rm int}(\tau)=F_{\rm int}(\tau,\phi)$. Nevertheless, as we will show now, the COIN method [22,23] is especially

suitable to reconstructing molecular vibrational wave packets.

A. Inversion method

For definiteness, we assume that the relative phase ϕ is uniformly distributed in the interval $[0,2\pi)$, that is, that each time the experiment is run at some fixed delay τ, the phase ϕ takes on an arbitrary value between 0 and 2π.

From Eqs. (6) and (9) we find that in the case of wave packet cross interferometry the fluctuations

$$\Delta F_{\rm tot}^2(\tau)\equiv\overline{F_{\rm tot}^2(\tau)}-\overline{F_{\rm tot}(\tau)}^2\equiv\Delta F_{\rm int}^2(\tau) \tag{23}$$

around the mean value $\overline{F_{\rm tot}(\tau)\equiv F_r}+F_o$ of the total signal are given by

$$\Delta F_{\rm int}^2(\tau)=2\left|\sum_n \tilde{a}_n\tilde{b}_n^* e^{-i\omega_n\tau}\right|^2$$

$$=2\sum_{n,m}\tilde{a}_n\tilde{a}_m^*\tilde{b}_n^*\tilde{b}_m e^{-i(\omega_n-\omega_m)\tau}. \tag{24}$$

Hence the signal $\Delta F_{\rm int}^2(\tau)$ contains *all* the phase information about the object wave packet embodied in the a_n coefficients.

For the purpose of reconstructing the coefficients $\tilde{a}_n$ from the measured quantity $\Delta F_{\rm int}^2(\tau)$ we join together the n and m indices to a single index $k=(n,m)$. Following our previous approach described in the last section we measure the fluctuations $\Delta F_{\rm int}^2(\tau)$ at discrete times τ_ν, and write the resulting set of equations in matrix form

$$\Delta F_{\rm int}^2(\tau_\nu)=\sum_k e_{\nu,k}\tilde{x}_k, \tag{25}$$

with the unknown coefficients

$$\tilde{x}_k\equiv\tilde{a}_n\tilde{a}_m^*=\tilde{x}_{n,m} \tag{26}$$

and the known matrix

$$e_{\nu,k}\equiv 2\tilde{b}_n^*\tilde{b}_m e^{-i(\omega_n-\omega_m)\tau_\nu}. \tag{27}$$

As in Refs. [14,15], we face the problem that the matrix $e_{\nu,k}$ as defined in Eq. (27) cannot be inverted, since it contains a number of columns, explicitly the $n\equiv m$ columns, which are composed of a *single* number. This is due to the fact that for $n\equiv m$ the phase of the exponential is always zero *independent* of the delay τ_ν. As a result, $e_{\nu,k}$ is a singular matrix.

One can solve this problem [14,15] by subtracting all diagonal terms with $n\equiv m$ from Eq. (25),

$$S(\tau_\nu)\equiv\Delta F_{\rm int}^2(\tau_\nu)-2\sum_n|\tilde{a}_n|^2|\tilde{b}_n|^2. \tag{28}$$

The second term can be derived from the observed signal $\Delta F_{\rm int}^2(\tau_\nu)$ by integrating the measured fluctuations $\Delta F_{\rm int}^2(\tau_\nu)$ over a single vibrational period of the excited wave packet,

$$I\equiv\int_0^{T_{\rm vib}}d\tau\Delta F_{\rm int}^2(\tau)=2\sum_{n,m}\tilde{a}_n\tilde{a}_m^*\tilde{b}_n^*\tilde{b}_m\int_0^{T_{\rm vib}}d\tau e^{-i(\omega_n-\omega_m)\tau}. \tag{29}$$

For a weakly anharmonic potential the Dunham expansion

$$\omega_n=\omega_{\bar{n}}+\frac{2\pi}{T_{\rm vib}}(n-\bar{n})\pm\frac{2\pi}{T_{\rm rev}}(n-\bar{n})^2\pm\cdots \tag{30}$$

yields in this case a revival time $T_{\rm rev}$, which is much larger than the vibrational period $T_{\rm vib}$,

$$T_{\rm rev}\gg T_{\rm vib}. \tag{31}$$

With the help of this expansion we find, for the energy difference,

$$\omega_n-\omega_m\equiv\frac{2\pi}{T_{\rm vib}}(n-m)\pm\cdots. \tag{32}$$

Since in Eq. (29) the delay τ is of the order of $T_{\rm vib}$, we can neglect higher-order terms in the exponent and find

$$I\simeq 2\sum_{n,m}\tilde{a}_n\tilde{a}_m^*\tilde{b}_n^*\tilde{b}_m\int_0^{T_{\rm vib}}d\tau e^{-i(2\pi/T_{\rm vib})(n-m)\tau}, \tag{33}$$

which reduces with the help of the representation

$$\delta_{n,m}=\frac{1}{T_{\rm vib}}\int_0^{T_{\rm vib}}d\tau e^{-i(2\pi/T_{\rm vib})(n-m)\tau} \tag{34}$$

for the Kronecker delta $\delta_{n,m}$ to

$$I\simeq 2T_{\rm vib}\sum_n|\tilde{a}_n|^2|\tilde{b}_n|^2. \tag{35}$$

Now the set of equations

$$S(\tau_\nu)\simeq\Delta F_{\rm int}^2(\tau)-\frac{I}{T_{\rm vib}}=\sum_{\substack{k=(n,m)\\ n\neq m}} e_{\nu,k}\tilde{x}_k \tag{36}$$

can be numerically inverted to yield the coefficients $\tilde{x}_k\equiv\tilde{a}_n\tilde{a}_m^*$ for which, via Eq. (10), one obtains the products $x_k\equiv a_n a_m^*=x_{n,m}$ for $n\neq m$.

By squaring the modulus of $x_{n,m}$ and summing over all $m\neq n$ we find

$$\sum_{m\neq n}|x_{n,m}|^2=|a_n|^2\sum_{m\neq n}|a_m|^2\equiv|a_n|^2(1-|a_n|^2), \tag{37}$$

where in the last step we have used the normalization condition $\Sigma_m|a_m|^2\equiv 1$. Hence the solution of the quadratic equations

$$|a_n|^4-|a_n|^2+\sum_{m\neq n}|x_{n,m}|^2=0 \tag{38}$$

yields $|a_n|$. Here, we only use the solution, which lies in the range $0\leqslant|a_n|^2\leqslant 1$.

To find the *phases* of the $\{a_n\}$ coefficients, we note that this set of complex-valued numbers is only determined up to

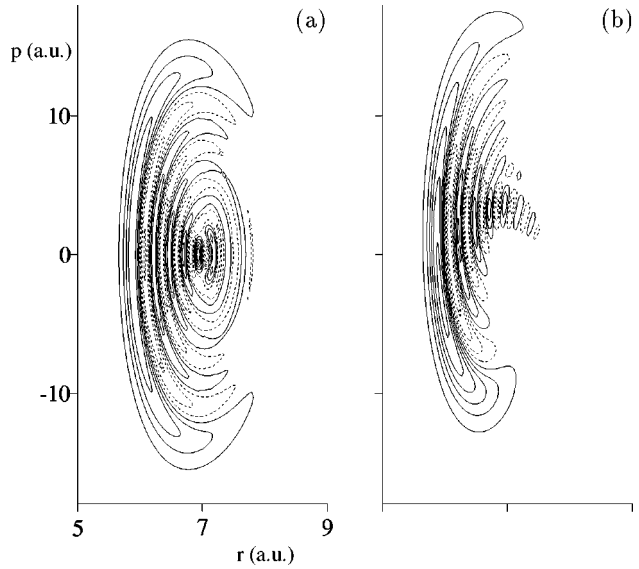

FIG. 7. Effect of a linear chirp in the exciting laser pulse on the resulting wave packet. In (a) and (b) we show Wigner functions of states excited by Gaussian pulses of duration $\Delta_t = 0.2T_{\rm vib}$. In (a), the pulse contains no chirp, whereas in (b) a linear chirp with rate $\alpha = 3/\Delta_t^2$ is employed. The chirp leads to a nontrivial distortion of the Wigner function.

a *common* phase factor. Fixing, say, a_{n_0}, to be real and positive, the phases of all the other coefficients a_n are given as

$$\arg[a_n] \equiv \arg[x_{n,n_0}]. \tag{39}$$

B. Example: Reconstruction of a ''chirped'' state

We demonstrate the above procedure for the case of the object wave packet excited by a linearly chirped pulse with envelope

$$\mathcal{E}(t) = \mathcal{E}_0 \exp\left(-\frac{t^2}{2\Delta_t^2} + i\alpha t^2 \right). \tag{40}$$

The use of chirped pulses in the field of coherent control has been investigated theoretically in detail by many authors [51–53]. Recently, experiments on quantum control with chirped pulses have been successfully performed [27,54,28].

Using first-order perturbation theory we find the probability amplitudes

$$a_n = \mathcal{N}\langle n|g\rangle \exp\left(-\frac{\Delta_n^2 \Delta_t^2}{2 + 8\alpha^2 \Delta_t^4} \right) \exp\left(-i \frac{\Delta_n^2 \alpha \Delta_t^4}{1 + 4\alpha^2 \Delta_t^4} \right), \tag{41}$$

where $\mathcal{N}$ is a constant. We see that an increase in the chirp factor α increases the width of the a_n distribution while introducing an additional phase factor. In Figs. 7(a) and 7(b) we show the Wigner functions for the state, Eq. (41), for the two different values $\alpha = 0$ and $\alpha = 3/\Delta_t^2$, respectively ($\Delta_t = 0.2T_{\rm vib}$). Thus, the chirp not only shifts the center of the Wigner function to positive momentum values, but also distorts considerably its internal structure. The state used for the reconstruction shown in Fig. 7(b), which has a rather complicated Wigner function, poses quite a challenge .

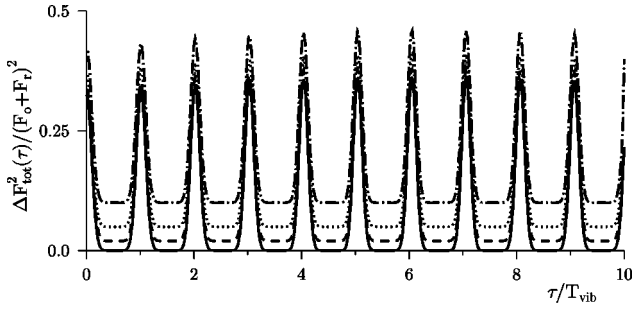

FIG. 8. COIN hologram of the ''chirped'' state shown in Fig. 7 (b). The hologram shows the total fluorescence fluctuations for different values of the system noise ΔF_s^2. The solid, dashed, dotted, and dashed-dotted lines correspond to the noise intensities $\Delta F_s^2/(F_o + F_r)^2 = 0$, 0.02, 0.05, and 0.1, respectively.

In our numerical simulation of quantum state holography for an unstable interferometer we again allow for experimental noise. In this case, the noise leads to an additional contribution ΔF_s^2 to the total fluorescence fluctuations $\Delta F_{\rm tot}^2(\tau)$. For simplicity, we treat this ''system noise'' as independent of the delay τ. In addition, we assume that the interference fluctuations $\Delta F_{\rm int}^2(\tau)$ and the system noise ΔF_s^2 are statistically independent and therefore simply add up to the total fluctuations as

$$\Delta F_{\rm tot}^2(\tau) = \Delta F_{\rm int}^2(\tau) + \Delta F_s^2 . \tag{42}$$

For the simulation we therefore replace $\Delta F_{\rm int}^2(\tau)$ in Eq. (36) by $\Delta F_{\rm tot}^2(\tau)$ as given in Eq. (42), sampled at 400 equally spaced data points at the discrete values τ_ν between $\tau = 0$ and $\tau = 10T_{\rm vib}$.

Figure 8 shows the total fluorescence fluctuations $\Delta F_{\rm tot}^2(\tau)$ for different values of the system noise ΔF_s^2 for the ''chirped'' state shown in Fig. 7(b). As the reference state we have used the ground state $|g\rangle$. We find an oscillating function with a period of about $T_{\rm vib}$, reflecting the quasiclassical oscillation of the wave packet to be reconstructed. In contrast to Fig. 4, no rapid oscillations with the optical frequency ω_L are present. We find that the envelope of the oscillations changes only slowly in time, thereby justifying the harmonic approximation in Eq. (33) for a single period.

In Fig. 9 we display the contour lines of reconstructed Wigner functions of the ''chirped'' state shown in Fig. 7(b). Here, we study the fidelity of the reconstruction for different values of additional system noise. In Fig. 9(a) where we use the value $\Delta F_s^2 = 0.02(F_o + F_r)^2$, an excellent agreement with the exact Wigner function is achieved. This reflects itself by the large fidelity parameter $o = 0.98$. Even in Figs. 9(b) and 9(c) where we increase the system noise to $\Delta F_s^2 = 0.05(F_o + F_r)^2$ and $\Delta F_s^2 = 0.1(F_o + F_r)^2$, respectively, one finds a good agreement between the exact and the reconstructed states, as evidenced by the fidelity parameters $o = 0.96$ and $o = 0.90$, respectively.

C. Case of a highly anharmonic potential

In the last section we have assumed that the wave packet only slightly changes its shape after *one* period which justifies the approximation in Eq. (33). This has allowed us to

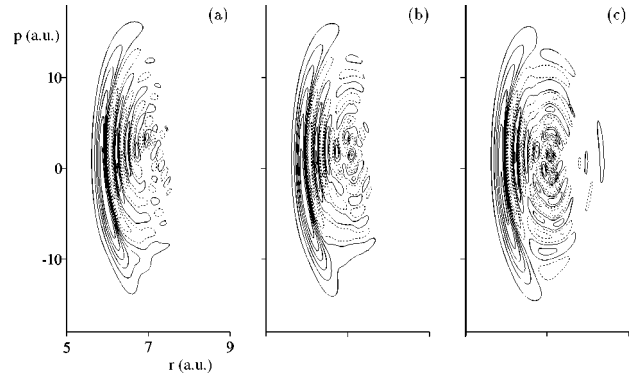

FIG. 9. Quantum-state holography of the ''chirped'' state displayed in Fig. 7(b). (a), (b), and (c) correspond to the dashed, dotted, and dashed-dotted curves in Fig. 8, respectively. We emphasize that even in the presence of large measurement errors the reconstructed Wigner functions still contain the main nontrivial features of the exact Wigner function.

subtract the diagonal terms from the fluctuations $\Delta F^2_{\rm int}(\tau)$ which removes the singularities in the matrix $e_{\nu,k}$, Eq. (27).

For a highly anharmonic potential, this approximation is not valid. In this case one has to look for a different method to find the diagonal terms. One possibility is to apply our method of quantum state holography to reconstruct the moduli $|a_n|^2$ and $|b_n|^2$ from an *autointerferometric* setup. Another possibility is to measure in addition to the fluctuations of the total (time- and frequency-*integrated*) fluorescence fluctuations $\Delta F^2_{\rm int}(\tau_\nu)$ the dispersed (frequency-*resolved*) fluorescence [14] of the object and the reference wave packet, respectively: The dispersed fluorescence

$$F_{\rm disp}(\omega)=\mathcal{F}\sum_{n,f}|\langle f|n\rangle|^2|a_n|^2\omega^4_{n,f}\delta_{\omega,\omega_{n,f}} \qquad (43)$$

of the wave packet Eq. (41) for $\alpha=3/\Delta_t^2$ is shown in Fig. 10. Here, we neglect the finite widths of the spectral lines. The peaks in this graph correspond to all those terms in the sum in Eq. (43), which have nonvanishing probabilities $|a_n|^2$ together with nonvanishing Franck-Condon factor $|\langle f|n\rangle|^2$. Hence the heights of these peaks directly yield the coefficients $|a_n|^2$.

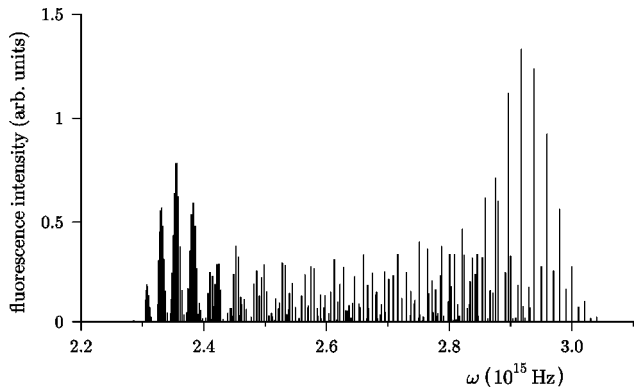

FIG. 10. Frequency-resolved fluorescence $F_{\rm disp}(\omega)$ of the ''chirped'' wave packet.

V. SUMMARY AND FURTHER APPLICATIONS OF THE METHOD

In this paper we propose the method of *quantum-state holography* to measure the quantum state of a vibrational wave packet in a molecule excited by a femtosecond laser pulse. Our technique is based on wave packet cross interferometry. This allows us to read out this state with the help of a known reference wave packet similar as in ordinary optical holography. The reference wave packet is excited by a second probe pulse which is delayed in time with respect to the pump pulse. By recording the subsequent incoherent fluorescence as a function of the delay between the two laser pulses, one obtains the cross interferogram which reflects the interference between the two wave packets. In contrast to autointerferograms, for which two identical wave packets are used, cross interferograms are phase sensitive and hence contain all the necessary information for reconstructing the complex wave function of the unknown wave packet in its moduli and phases.

We have demonstrated the feasibility of our method by numerically simulating realistic quantum-state holography experiments. We have considered the case of a stable interferometer as well as a noisy COIN interferometer and have tested the robustness of the method by including simulated measurement errors. Our numerical studies clearly demonstrate the feasibility of quantum-state holography for unstable interferometers even in the presence of additional system noise. One can subtract this additional noise contribution from the measured signal by separately exciting the object or the reference wave packet, which yields directly the system noise.

COIN holography is less sensitive to experimental noise than the linear variant of the method. However, the price one has to pay for this is that the inversion of the system of equations (36) is numerically less stable than the inversion of the corresponding system of equations (14) for the case of a stable interferometer. This is due to the fact that in Eq. (36) the unknown coefficients $\tilde{a}_n$ enter *bilinearly*, whereas in Eq. (14) they enter *linearly*.

We emphasize that in contrast to *emission tomography* [13] our technique does not rely on weakly anharmonic potentials and is capable of recovering even highly nonclassical features of quantum states. Moreover, this method also allows us to reconstruct the quantum state of an electronic wave packet in Rydberg atoms. Indeed, after the present paper was prepared for publication, we became aware of an experiment [48] in which a variant of the COIN holography scheme was applied to a full amplitude and phase reconstruction of a Rydberg wave packet. A related scheme for the reconstruction of engineered atomic wave functions via phase-sensitive measurements was suggested recently in [55].

We conclude by noting that quantum-state holography might also be a powerful tool to determine the spectral amplitudes and phases of ultrashort laser pulses: Here, we use the molecule as a ''grating'' to chop the unknown pulse into its spectral amplitudes and phases which we later read out with the help of a simple reference pulse. This technique might be complimentary to the established method of ''frequency-resolved optical gating'' (FROG) [56,57].

ACKNOWLEDGMENTS

C.L. thanks the Deutsche Forschungsgemeinschaft for its support and acknowledges the warm hospitality during his stay at the Weizmann Institute of Science, Rehovot. M.S. and I.A. wish to acknowledge support from the Minerva Foundation, the Israel Science Foundation, the James Franck Program, and the U.S.-Israel Binational Science Foundation. M.S. also thanks U.S. Office of Naval Research for its support. The work was supported in part by the Israel Ministry of Absorption and the Center for Absorption of Scientists. We are grateful to P. Bucksbaum for sending us a copy of Ref. [48] prior to publication.

[1] For the most recent overview, see, for example, the special issue on quantum state preparation and measurement, edited by W. Schleich and M. Raymer, J. Mod. Opt. **44**, 2021 (1997).
[2] M. Freyberger, P. Bardroff, C. Leichtle, G. Schrade, and W. Schleich, Phys. World **10** (11), 41 (1997).
[3] D. Leibfried, T. Pfau, and C. Monroe, Phys. Today **51** (4), 22 (1998).
[4] D.-G. Welsch, W. Vogel, and T. Opatrny, in *Progress in Optics*, edited by E. Wolf (North-Holland, Amsterdam, in press).
[5] M. Freyberger, Phys. Lett. A **242**, 193 (1998).
[6] J. R. Ashburn, R. A. Cline, C. D. Stone, P. J. M. van der Burgt, W. B. Westerveld, and J. S. Risley, Phys. Rev. A **41**, 4885 (1989); **41**, 2407 (1990).
[7] N. G. Walker and J. E. Carroll, Opt. Quantum Electron. **18**, 355 (1986).
[8] J. W. Noh, A. Fougeres, and L. Mandel, Phys. Rev. Lett. **67**, 1426 (1991).
[9] D. T. Smithey, M. Beck, M. G. Raymer, and A. Faridani, Phys. Rev. Lett. **70**, 1244 (1993).
[10] S. Schiller, G. Breitenbach, S. F. Pereira, T. Müller, and J. Mlynek, Phys. Rev. Lett. **77**, 2933 (1996).
[11] D. Leibfried, D. M. Meekhof, B. E. King, C. Monroe, W. M. Itano, and D. J. Wineland, Phys. Rev. Lett. **77**, 4281 (1996).
[12] C. Kurtsiefer, T. Pfau, and J. Mlynek, Nature (London) **386**, 150 (1997).
[13] T. J. Dunn, I. A. Walmsley, and S. Mukamel, Phys. Rev. Lett. **74**, 884 (1995).
[14] M. Shapiro, J. Chem. Phys. **103**, 1748 (1995).
[15] M. Shapiro, Chem. Phys. **207**, 317 (1996).
[16] U. Leonhardt and M. G. Raymer, Phys. Rev. Lett. **76**, 1985 (1996).
[17] I. A. Walmsley, T. J. Dunn, and J. N. Sweetser, in *Proceedings of ''Coherence and Quantum Optics VII,''* edited by J. H. Eberly, L. Mandel, and E. Wolf (Plenum Press, New York, 1996), p. 73.
[18] U. Leonhardt, Phys. Rev. A **55**, 3164 (1997).
[19] L. Davidovich, M. Orszag, and N. Zagury, Phys. Rev. A **57**, 2544 (1998).
[20] I. Sh. Averbukh and N. F. Perelman, Phys. Lett. A **139**, 449 (1989); Sov. Phys. JETP **69**, 464 (1989).
[21] C. Leichtle, W. P. Schleich, I. Sh. Averbukh, and M. Shapiro, Phys. Rev. Lett. **80**, 1418 (1998).
[22] O. Kinrot, I. Sh. Averbukh, and Y. Prior, Phys. Rev. Lett. **75**, 3822 (1995)
[23] C. Leichtle, W. P. Schleich, I. Sh. Averbukh, and M. Shapiro, J. Chem. Phys. **108**, 6057 (1998).
[24] A. M. Weiner, J. P. Heritage, and R. N. Thurston, Opt. Lett. **11**, 153 (1986).
[25] A. M. Weiner, D. E. Leaird, G. P. Wiederbrecht, and K. A. Nelson, Science **247**, 1317 (1990).
[26] D. W. Schumacher, J. H. Hoogenraad, D. Pinkos, and P. H. Bucksbaum, Phys. Rev. A **52**, 4719 (1995).
[27] B. Kohler, V. Yakovlev, J. Che, J. L. Krause, M. Messina, K. R. Wilson, N. Schwentner, R. M. Whitnell, and Y. Yan, Phys. Rev. Lett. **74**, 3360 (1995).
[28] A. Assion, T. Baumert, J. Helbing, V. Seyfried, and G. Gerber, Chem. Phys. Lett. **259**, 488 (1996).
[29] D. Gabor, Proc. R. Soc. London, Ser. A **197**, 454 (1949).
[30] J. F. Christians and B. Broers, Phys. Rev. A **52**, 3655 (1995).
[31] N. F. Scherer, A. J. Ruggiero, M. Du, and G. R. Fleming, J. Chem. Phys. **93**, 856 (1990); N. F. Scherer, R. J. Carlson, A. Matro, M. Du, A. J. Ruggiero, V. Romero-Rochin, J. A. Cina, G. R. Fleming, and S. A. Rice, *ibid.* **95**, 1487 (1991); N. F. Scherer, A. Matro, L. D. Ziegler, M. Du, R. J. Carlson, J. A. Cina, and G. R. Fleming, *ibid.* **96**, 4180 (1992).
[32] M. W. Noel and C. R. Stroud, Jr., Phys. Rev. Lett. **75**, 1252 (1995).
[33] M. W. Noel and C. R. Stroud, Jr., Phys. Rev. Lett. **77**, 1913 (1996).
[34] V. Blanchet, M. A. Bouchene, O. Cabrol, and B. Girard, Chem. Phys. Lett. **233**, 491 (1995); V. Blanchet, C. Nicole, M. A. Bouchene, and B. Girard, Phys. Rev. Lett. **78**, 2716 (1997).
[35] W. H. Press, S. A. Teukolsky, W. T. Vetterling, and B. P. Flannery, *Numerical Recipes* (Cambridge University Press, Cambridge, England, 1992).
[36] I. Schmidt, Ph.D. thesis, Universität Kaiserslautern, 1987.
[37] B. R. Johnson, J. Chem. Phys. **67**, 4086 (1977).
[38] J. Janszky, A. V. Vinogradov, T. Kobayashi, and Z. Kiss, Phys. Rev. A **50**, 1777 (1994).
[39] I. A. Walmsley and M. G. Raymer, Phys. Rev. A **52**, 681 (1995).
[40] C. Monroe, D. M. Meekhof, B. E. King, and D. J. Wineland, Science **272**, 1131 (1996).
[41] M. Brune, E. Hagley, J. Dreyer, X. Maitre, A. Maali, C. Wunderlich, J. M. Raimond, and S. Haroche, Phys. Rev. Lett. **77**, 4887 (1996).
[42] M. Hillery, R. F. O'Connell, M. O. Scully, and E. P. Wigner, Phys. Rep. **106**, 121 (1984).
[43] B. Dutta, N. Mukunda, R. Simon, and A. Subramanian, J. Opt. Soc. Am. B **10**, 253 (1993).
[44] I. Sh. Averbukh and M. Shapiro, Phys. Rev. A **47**, 5086 (1993); D. G. Abrashkevich, I. Sh. Averbukh, and M. Shapiro, J. Chem. Phys. **101**, 9295 (1994).
[45] J. F. Christian, B. Broers, J. H. Hoogenraad, W. J. van der Zande, and L. D. Noordam, Opt. Commun. **103**, 79 (1993).
[46] L. D. Noordam, D. I. Duncan, and T. F. Gallagher, Phys. Rev. A **45**, 4734 (1992); B. Broers, J. F. Christian, J. H. Hoogenraad, W. J. van der Zande, and H. B. van den Linden van den Heuvell, Phys. Rev. Lett. **71**, 344 (1993); R. R. Jones, C. S. Raman, D. W. Schumacher, and P. H. Bucksbaum, *ibid.* **71**,

2575 (1993); B. Broers, J. F. Christian, and H. B. van den Linden van den Heuvell, Phys. Rev. A **49**, 2498 (1994); G. M. Lankhuijzen and L. D. Noordam, *ibid.* **52**, 2016 (1995).

[47] J. Wals, H. H. Fielding, J. F. Christian, L. C. Snoek, W. J. van der Zande, and H. B. van den Linden van den Heuvell, Phys. Rev. Lett. **72**, 3783 (1994); J. Wals, H. H. Fielding, and H. B. van den Linden van den Heuvell, Phys. Scr. **T58**, 62 (1995).

[48] T. C. Weinacht, J. Ahn, and P. H. Bucksbaum, Phys. Rev. Lett. **80**, 5508 (1998).

[49] A. Tortschanoff, K. Brunner, Ch. Warmuth, and H. F. Kauffmann (unpublished).

[50] V. Szocs and H. F. Kauffmann, J. Lumin. **76**, 145 (1998).

[51] S. Ruhman and R. Kosloff, J. Opt. Soc. Am. B **7**, 1748 (1990).

[52] S. Chelkowski, A. D. Bandrauk, and P. B. Corkum, Phys. Rev. Lett. **65**, 2355 (1990).

[53] B. Amstrup, J. D. Doll, R. A. Sauerbrey, G. Szabó, and A. Lörincz, Phys. Rev. A **48**, 3830 (1993).

[54] C. J. Bardeen, Q. Wang, and C. V. Shank, Phys. Rev. Lett. **75**, 3410 (1995).

[55] X. Chen and J. A. Yeazell, Phys. Rev. A **56**, 2316 (1997).

[56] R. Trebino and D. J. Kane, J. Opt. Soc. Am. A **10**, 1101 (1993).

[57] K. W. DeLong, R. Trebino, and D. J. Kane, J. Opt. Soc. Am. B **11**, 1595 (1994).